EARTHQUAKE ENGINEERING AND STRUCTURAL DYNAMICS
Earthquake Engng Struct. Dyn. 2003; **32**:2197–2219 (DOI: 10.1002/eqe.323)

Near-fault spatial variation in strong ground motion due to rupture directivity and hanging wall effects from the Chi-Chi, Taiwan earthquake

Khosrow T. Shabestari[1,*,†] and Fumio Yamazaki[2]

[1]*Earthquake Disaster Mitigation Research Center, National Research Institute for Earth Science and Disaster Prevention, 4F Human Renovation Museum, 1-5-2 Kaigan-dori, Wakahama, Chuo-Ku, Kobe 651-0073, Japan*
[2]*Institute of Industrial Science, University of Tokyo, Tokyo 153-8505, Japan*

SUMMARY

Damaging earthquakes feature large variations in the spatial ground motion distribution mainly due to source complexity, radiation pattern, and site conditions. In this study, we tried to capture the hanging wall and rupture directivity effects from the 1999 Chi-Chi, Taiwan earthquake ($M_w = 7.6$), which provides the largest acceleration data set since the strong-motion seismology studies began. First, the event-specific attenuation relations of strong-motion parameters for the near-field, hanging wall and footwall sites were developed. Then an empirical hanging wall model for peak ground acceleration (PGA) was introduced to get the residuals from the obtained attenuation relationships. The new empirical model for the PGA on the hanging wall indicates 46% to 50% higher values than the predicted means over the near-field distance ranges. Finally, a period-dependent empirical spectral amplitude factor model representing the directivity effects for the dip-slip faulting system was developed using the Somerville *et al.* directivity model. The proposed model shows a larger spectral amplification factor than the result of the previous study. During the Chi-Chi earthquake, the maximum spectral directivity factors have been registered in the up-dip region, located around the surface exposure of the Chelungpu fault, in the range of 1.1 to 1.3 for the structural periods from 0.6 s to 5.0 s. Since the proposed spectral directivity factor was derived from the residual function of the single event without any influence of inter-event variability, the model is magnitude- and distance-independent. Hence the result can be easily implemented into attenuation relations, seismic hazard assessment, and building code revision studies for the regions with a dip-slip faulting. Copyright © 2003 John Wiley & Sons, Ltd.

KEY WORDS: 1999 Chi-Chi earthquake; attenuation relation; strong-motion record; hanging wall; directivity; dip-slip faulting

1. INTRODUCTION

Near-fault earthquake ground motion can be strongly enhanced relative to more distant sites due to the proximity to the source and the presence of directivity effects caused by coherent, long-period velocity pulses [1]. Recent studies on near-fault ground motion accentuate the

* Correspondence to: Khosrow T. Shabestari, Earthquake Disaster Mitigation Research Center, National Research Institute for Earth Science and Disaster Prevention, 4F Human Renovation Museum, 1-5-2, Kaigan-dori, Wakahama, Chuo-Ku, Kobe 651-0073, Japan.
† E-mail: khosrow@edm.bosai.go.jp

Received 8 July 2002
Revised 3 December 2002
Accepted 24 March 2003

importance of these prominent characteristics to mitigate possible recurrent damage due to earthquakes in urban areas [2, 3]. Realistic capturing and modeling of near-source strong motion are affected by many factors such as geometry and type of faulting, local soil conditions, 3D basin effects, topographic relief, and strong underground heterogeneity [4, 5]. From previous damaging earthquakes, numerous studies on near-source ground motion have asserted the potential severity of long-period pulses, which require very high drift demands for flexible structures [5–12]. The recent emphasis on the importance of coherent, long-period pulses in near-source ground motions has sparked concern about the response of engineered structures to such motions. This interest mostly came from the observations, such as widespread casualties and structural damage, and severe ground motion recordings, from the recent events such as the 1994 Northridge, the 1995 Hyogoken-Nanbu (Kobe), and the 1999 Chi-Chi, Taiwan earthquakes [5, 13].

The Rapid development of strong-motion instrumentation has provided a more accurate and efficient modeling of this important near-fault feature. The Chi-Chi, Taiwan earthquake on 21 September 1999, with moment magnitude of 7.6, was the most destructive earthquake to strike this island since 1935 [14]. Based on fault plane solutions and field investigations, this event is characterized by a low-angle thrust faulting system named the Chelungpu fault [15]. The main rupture propagated from the south to the north with a length of 100 km and width of 40 km, with the maximum slip distribution (asperity) of 9 m that concentrated in the northern part of the Chelungpu fault [16]. The 1999 Chi-Chi earthquake provides the largest acceleration data set since the strong-motion seismology studies began [17]. The strong ground motion records from this event provide us with an unusual opportunity to investigate the characteristics of near-source ground motion.

In this study we capture near-fault ground motion phenomena, the rupture directivity and hanging wall effects, directly resulting from the fault geometry as well as the dynamic rupture process during the Chi-Chi earthquake [18, 19]. Many researchers have developed empirical relationships to estimate spatial ground motion distribution in terms of magnitude, distance, local site conditions, and other variables using the data from specific tectonic settings, or worldwide [20–22]. Since we have a large number of near-field records from the 1999 Chi-Chi earthquake, the event-specific attenuation characteristics of the near-field, hanging wall and footwall regions are examined. Then we present an empirical approach to evaluate the systematic difference in peak ground acceleration (PGA) at the hanging wall and footwall stations, using the residuals from the Chi-Chi earthquake-specific attenuation relation. Furthermore, the frequency-dependent directivity effect, which results from the dip-slip faulting system and rupture propagation toward recording sites, is proposed in terms of the spectral amplification factor. The results from the proposed spectral amplitude ratios as well as the hanging wall model are compared with the results from the previous studies by Somerville *et al.* [1] and Abrahamson and Somerville [18]. Since the proposed spectral directivity factor model is magnitude- and distance-independent, the result might be employed to other attenuation relations as well as for building code revision studies for shallow large-magnitude events with large surface breaks.

CHARACTERISTICS OF THE NEAR-FAULT STRONG MOTION DATA SET

Since some of the near-fault ground motions are characterized by long-period, pulse-like time histories, an appropriate baseline correction scheme was used to preserve these important

near-field motion characteristics [23]. In order to demonstrate the characteristics of near-fault strong motion from the large crustal earthquake, the PGA and the peak ground velocity (PGV) are defined as the maximum of the resultant of two horizontal components between 0° and 360° (denoted by PGA_R and PGV_R), and they were calculated for all the near-fault stations. Figure 1 demonstrates the location of the epicenter, the Chelungpu fault surface trace, and the maximal velocity direction along the fault surface. The difference in the amplitudes of the strike-normal and strike-parallel components, which are very important characteristics of the near-fault ground motion records [1, 13], is observed as normal to the fault strike for both the hanging wall and footwall stations with the opposite directions.

Figure 2(a) shows the relationship between PGA_R and PGV_R for the records obtained in the Chi-Chi earthquake. As shown in the figure, at the TCU052 (Taichung) and TCU068 (Shihgang) stations in the northeast hanging-wall side of the Chelungpu fault, the PGV was as large as 266 cm/s and 384 cm/s, respectively. However, at the TCU129 (Mingchien) station in the southern footwall side of the fault, the PGV was observed as 79 cm/s while its PGA reached more than 980 cm/s^2. However, later, Wen *et al.* [24] demonstrated that the high PGA recorded at the TCU129 station was due to the concrete recording pier effect, thus, we excluded this record from our data set. In spite of these large PGV values, structural damage around the instruments were not too severe. Initially, this was explained by the fact that the period of the pulse was much larger than the natural periods of the structures nearby. According to a dynamic source simulation and 3D velocity structure inversion around the Chelungpu fault area, in the northern part the rupture propagation reached the surface with a slow velocity compared to that in the southern part of the fault [4, 25]. However, the long-period coherent pulse of the rupture front (directivity) was included in the records in the near-fault region [26]. Since the PGV is affected by such long-period contents, it is sometimes not a reliable parameter to correlate with structure damage. In Japan, the JMA intensity has been used for many years as a measure of strong shaking in addition to PGA. It was originally determined by the human judgment of JMA officers. But, in the early 1990s, JMA began moving to an instrumental seismic intensity (I_{JMA}) and away from human judgment. In 1996, the JMA intensity scale was revised and a large number of seismometers measuring the JMA intensity were deployed throughout Japan [27]. The instrumental seismic intensity, which is obtained from the three-component acceleration records, is currently broadcast through public TV and radio soon after an earthquake occurs. For disaster management agencies in Japan, it is used as the most important index to estimate structural damage due to earthquakes [28]. The details of the JMA seismic intensity algorithms are given by Shabestari and Yamazaki [29].

The spectrum intensity (SI) is another important strong motion index that is used to estimate the structural damage due to earthquakes. In Japan, the SI value is used for the index to shut-off natural gas supplies after a strong earthquake. Based on the seismic records and damage caused to gas pipes in the vicinity of instruments in the 1995 Kobe earthquake, an SI value of 60 cm/s was set as the level of shaking for mandatory shut-off of city gas supplies. Following this criterion, the Tokyo Gas Co., Ltd developed SI sensors [30] that calculate the SI value within the sensor using acceleration records. Recently, the deployment of new SI-sensors has begun in the Tokyo metropolitan area, and the super-dense seismic monitoring system (SUPREME) with 3700 new SI sensors will be completed by 2007 [31]. The spectrum intensity is calculated as the area under the velocity response spectrum with a damping ratio of 0.2 between the period of 0.1 s and 2.5 s [30, 32]. In this study the SI values are computed for each 1-degree interval on the horizontal plane and the maximum one of them is defined

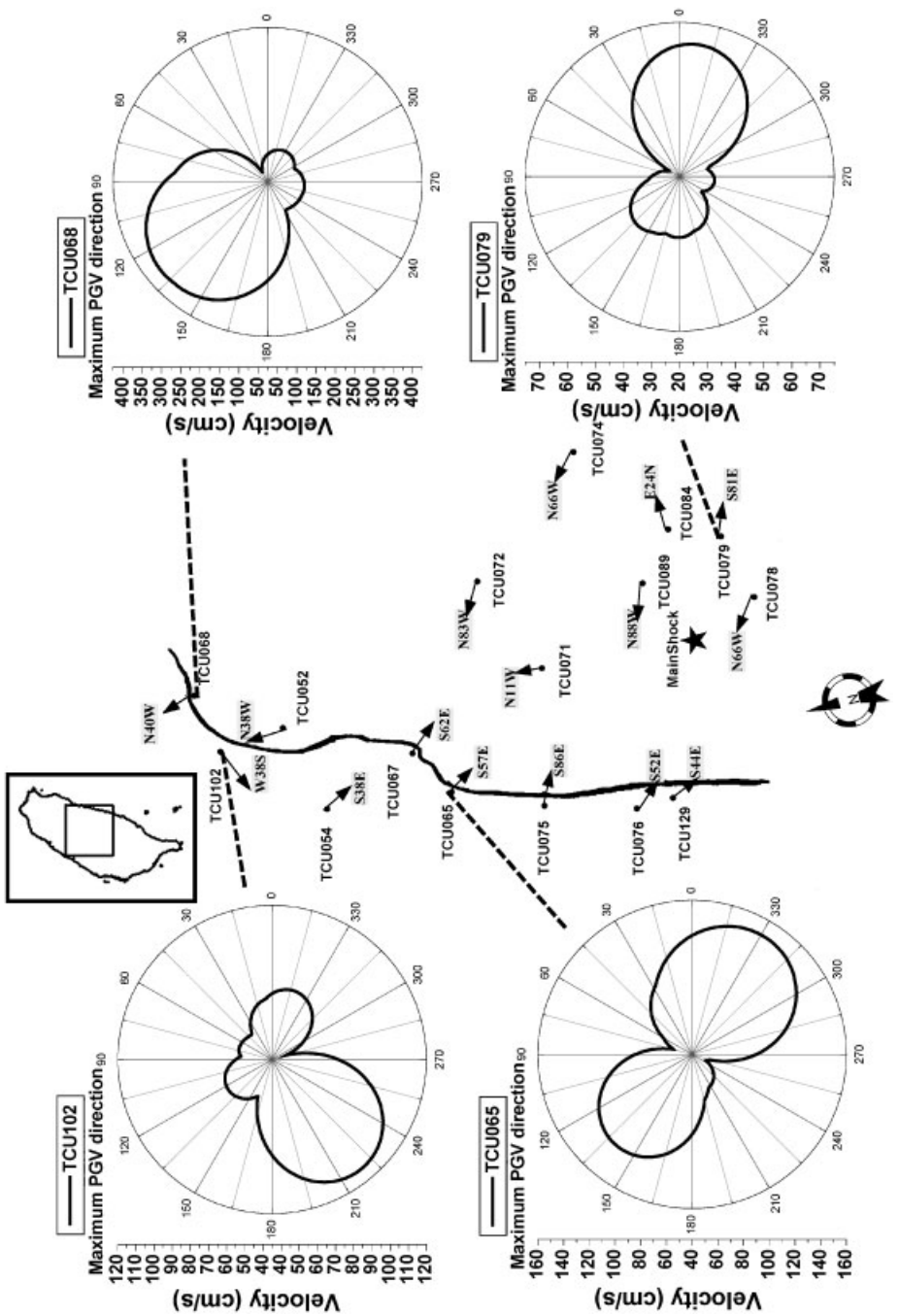

Figure 1. Map showing the epicenter (star) and surface trace of the Chelungpu fault in the 1999 Chi-Chi, Taiwan earthquake. Location of near-fault stations with the maximal velocity direction and rotated maximum PGV for some stations.

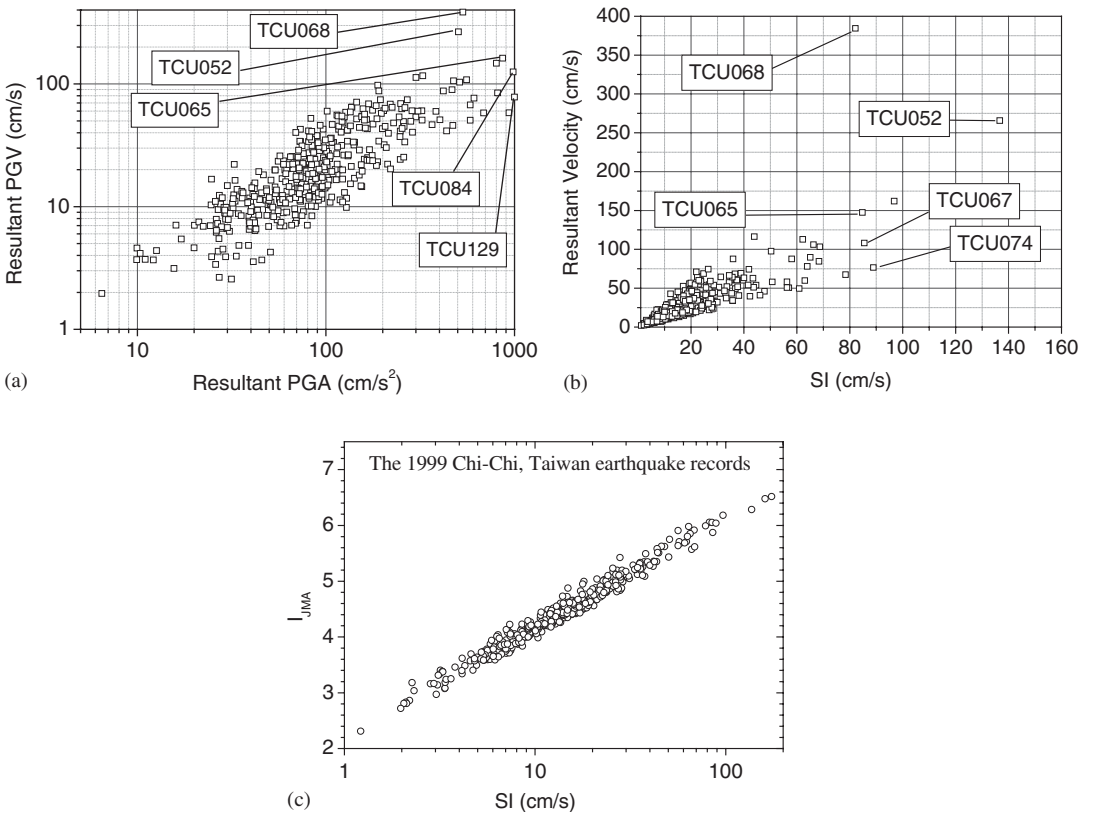

Figure 2. Relationships between resultant PGV and (a) resultant PGA and (b) the spectral intensity (SI), and (c) relationship between I_{JMA} and SI, for the 1999 Chi-Chi earthquake.

as the SI. The relationship between the SI and PGV is shown in Figure 2(b) for the Chi-Chi earthquake. Although the SI and PGV are in a linear relationship for most cases [32], a large difference is observed for some near-fault stations (e.g. TCU068, TCU052) in this event. This observation can be explained by the fact that the long-period contents larger than 2.5 s are dominant in these records. Since the SI is obtained as the average amplitude of the velocity response between 0.1 s and 2.5 s, it does not reflect such long-period contents. On the contrary, good correlation between I_{JMA} and SI has been observed for the Chi-Chi earthquake (Figure 2(c)).

CHI-CHI EARTHQUAKE-SPECIFIC ATTENUATION RELATIONSHIPS

Since the 1999 Chi-Chi, Taiwan earthquake was well recorded, the event-specific attenuation relations for PGA as well as other strong-motion indices such as PGV, SI, and I_{JMA} were derived for all the selected records within the shortest distance of 60 km to the seismogenic

part of the fault plane [33] (including recording stations off the ends of the Chelungpu fault, with the 110 acceleration records). The final data sets for the hanging wall and footwall stations (excluding sites off the end of the fault rupture) contain 37 and 66 pairs of the three-component acceleration records, respectively. The closest distance from each recording station to the seismogenic rupture plane is calculated using the USGS fault plane solution [15] (Table I). Then the 1999 Chi-Chi earthquake specific attenuation relationships were developed considering anelastic attenuation and geometric spreading for the ground motion parameters.

Regression model

The attenuation model considering the near-source saturation effect for the strong ground motion indices is given by

$$y = b_0 + b_1 r + b_2 \log_{10}(r + d) + \varepsilon \tag{1}$$

in which y is $\log_{10}$PGA, $\log_{10}$PGV, $\log_{10}$SI, or the I_{JMA}, r is the closest distance to the seismogenic part of the fault plane, b_i are the regression coefficients to be determined, d is the near-source saturation effect in kilometers, and ε represents the error term. The terms $b_1 r$ and $b_2 \log_{10}(r + d)$ represent anelastic attenuation and geometric spreading, respectively. The near-source saturation term (d) is applied only for the geometric spreading term. This is because in the near-source region, anelastic attenuation is negligible compared with geometric spreading. Since the near-source data used in this study is from a single earthquake, the saturation effect term (d) was assumed to be constant. A non-linear least square analysis for the 1999 Chi-Chi, Taiwan earthquake was performed to obtain d. This was accomplished by the iteration to find d where the sum of squares of errors was minimized. The error term is defined as the difference between the predicted ground motion parameters from Equation (1) for a trial value of d and the corresponding recorded ground motion indices.

Results of the regression analysis

The results of regression analysis for the ground motion parameters for this earthquake are given in Table II. Figure 3 shows the predicted $\mathrm{PGA_R}$, $\mathrm{PGV_R}$, SI, and I_{JMA} by the attenuation relationships for the hanging wall and footwall stations. Since the 1999 Chi-Chi earthquake provides a useful strong ground motion data set especially for the near-fault region, the near-source saturation effect (d) has been taken into account. However, since the near-field data in this study are limited to only one event, it is not possible to judge whether the records support the magnitude-independence of the saturation effect or not. The near-source attenuation characteristics of PGA have been studied by several researchers [33, 34]. Most of them constrained the near-field attenuation model assuming the peak ground acceleration near the fault rupture is magnitude-independent. The main reason for the differences on the d term obtained in this study and the other studies is referred to as the earthquake-to-earthquake component of the variability [35] and also the influence on the spatial distribution of the ground motion due to the radiation pattern from the source to the recording sites, located in the hanging wall and footwall regions. From Figure 3 it can be seen that the

Table I. Summary of the near-fault strong motion records analyzed for the development of hanging wall and directivity models. The calculated PGA and PGV are the resultant of the two horizontal components, recorded by the Central Weather Bureau (CWB) and the Central Mountain Strong-Motion Array (CMSMA) of Taiwan during the 1999 Chi-Chi earthquake.

No.	Station code	Latitude (°N)	Longitude (°E)	r_{epi} (km)	r_{seis} (km)	Soil type	PGA_R (cm/s^2)	PGV_R (cm/s)	SI (cm/s)	I_{JMA}	$Y\cos(\phi)$
Footwall stations											
1	CHY002	23.720	120.413	42.4	32.5	E	134.8	59.0	27.4	4.9	0.484
2	CHY004	23.602	120.175	70.2	56.6	E	101.0	23.2	12.0	4.4	0.346
3	CHY006	23.582	120.552	39.9	18.0	D	383.3	59.8	63.0	5.8	0.576
4	CHY024	23.758	120.607	22.8	13.1	D	307.6	60.1	39.7	5.3	0.592
5	CHY025	23.708	120.514	30.5	22.6	E	164.4	51.3	30.6	5.1	0.548
6	CHY026	23.799	120.412	40.1	33.1	E	80.9	41.4	16.6	4.5	0.479
7	CHY027	23.752	120.247	57.6	49.6	E	59.9	22.5	7.6	4.1	0.379
8	CHY028	23.633	120.606	32.1	12.1	D	864.7	162.0	96.8	6.2	0.594
9	CHY029	23.614	120.529	38.9	20.1	C	287.9	40.5	38.1	5.5	0.563
10	CHY032	23.580	120.294	60.1	44.2	E	97.1	25.0	20.5	4.7	0.412
11	CHY036	23.608	120.479	43.1	25.2	D	299.7	53.9	44.6	5.5	0.533
12	CHY076	23.638	120.222	63.8	51.5	E	92.6	28.6	10.7	4.3	0.369
13	CHY080	23.597	120.678	31.7	4.9	?	1128.9	150.1	174.1	6.5	0.599
14	CHY082	23.725	120.300	53.4	44.3	E	85.0	29.3	11.2	4.3	0.410
15	CHY092	23.792	120.478	33.6	26.3	E	101.6	60.0	23.0	4.8	0.525
16	CHY094	23.794	120.322	49.4	42.3	E	64.9	25.4	10.3	4.2	0.421
17	CHY101	23.686	120.562	30.9	17.1	D	474.7	106.1	66.3	5.6	0.577
18	CHY104	23.670	120.466	40.1	26.9	E	184.8	66.4	34.5	5.2	0.522
19	CHY111	23.791	120.227	48.8	44.6	E	82.2	20.4	13.8	4.2	0.367
20	CHY112	23.704	120.183	55.2	48.6	E	140.3	22.4	11.3	4.2	0.347
21	TCU049	24.180	120.690	37.0	7.2	D	322.4	60.4	34.9	5.2	0.600
22	TCU050	24.182	120.633	39.4	12.7	D	150.5	44.2	22.3	4.9	0.591
23	TCU051	24.161	120.652	36.5	10.9	D	244.6	53.9	28.6	5.2	0.596
24	TCU053	24.194	120.669	39.2	9.3	D	228.4	48.1	26.9	5.2	0.598
25	TCU054	24.162	120.675	35.7	8.6	D	196.7	57.4	34.5	5.1	0.599
26	TCU055	24.140	120.664	33.8	9.5	D	286.93	60.5	37.3	5.4	0.598
27	TCU056	24.159	120.624	37.6	13.7	D	166.1	43.1	24.5	5.0	0.589
28	TCU057	24.178	120.611	39.6	15.1	C	121.8	49.5	23.7	4.9	0.583
29	TCU059	24.269	120.564	51.2	20.4	D	176.8	61.1	34.5	5.2	0.558
30	TCU060	24.225	120.644	43.3	11.9	D	206.1	45.1	20.1	4.8	0.593
31	TCU061	24.136	120.549	39.7	21.1	D	160.0	50.8	25.7	4.9	0.555
32	TCU063	24.109	120.616	33.2	14.2	D	190.9	87.6	35.9	5.2	0.587
33	TCU064	24.346	120.610	57.1	16.1	D	127.3	58.8	23.8	4.8	0.574
34	TCU065	24.059	120.691	24.6	6.6	D	801.5	147.4	84.8	6.1	0.600
35	TCU067	24.092	120.720	26.8	4.3	D	556.6	108.2	85.5	5.9	0.598
36	TCU070	24.196	120.547	45.6	22.3	C	249.2	69.1	38.9	5.4	0.551
37	TCU075	23.986	120.678	18.4	7.4	D	326.5	116.4	43.9	5.5	0.600
38	TCU076	23.908	120.676	13.7	7.2	D	419.9	87.6	58.1	5.7	0.600
39	TCU082	24.148	120.676	34.2	8.5	D	262.5	64.2	35.6	5.3	0.599
40	TCU100	24.186	120.615	40.6	14.6	C	130.1	42.1	20.0	4.8	0.585
41	TCU101	24.242	120.710	43.3	5.7	D	270.3	74.3	41.9	5.4	0.599
42	TCU102	24.249	120.721	43.8	4.8	D	300.3	112.8	62.2	5.7	0.598
43	TCU103	24.310	120.716	50.7	6.2	D	168.5	68.8	24.8	5.0	0.599
44	TCU104	24.210	120.602	47.2	16.1	C	114.4	55.8	19.4	4.7	0.579
45	TCU105	24.239	120.560	48.6	20.7	C	135.1	45.5	19.3	4.7	0.557

Table 1 (*continued*)

No.	Station code	Latitude (°N)	Longitude (°E)	r_{epi} (km)	r_{seis} (km)	Soil type	PGA_R (cm/s^2)	PGV_R (cm/s)	SI (cm/s)	I_{JMA}	$Y \cos(\phi)$
46	TCU106	24.086	120.549	35.3	20.5	D	161.9	43.6	28.1	5.0	0.557
47	TCU107	24.264	120.539	35.4	21.7	D	145.4	51.8	37.6	5.1	0.543
48	TCU109	24.085	120.571	34.0	18.6	D	202.4	60.6	35.1	5.3	0.568
49	TCU110	23.962	120.570	26.0	18.1	E	188.4	97.6	50.3	5.4	0.572
50	TCU111	24.114	120.487	42.4	27.2	E	125.3	53.9	24.3	4.9	0.517
51	TCU112	24.056	120.424	43.9	33.4	E	83.26	52.4	17.1	4.5	0.476
52	TCU113	23.893	120.386	42.2	36.2	E	73.4	34.0	14.3	4.4	0.458
53	TCU115	23.960	120.47	35.4	28.2	E	115.9	54.9	22.9	4.8	0.512
54	TCU116	23.857	120.580	22.3	16.3	E	186.6	52.0	33.6	5.2	0.580
55	TCU117	24.133	120.460	45.9	30.1	E	136.7	65.0	31.3	5.1	0.498
56	TCU118	24.003	120.423	41.4	33.1	E	120.5	40.4	17.7	4.7	0.478
57	TCU119	23.924	120.312	50.1	43.9	E	66.1	25.6	12.8	4.2	0.410
58	TCU120	23.980	120.613	23.2	13.5	C	252.7	62.8	43.5	5.4	0.589
59	TCU122	23.813	120.610	20.0	13.1	D	257.6	49.4	36.8	5.3	0.591
60	TCU123	24.018	120.543	31.4	21.0	D	154.7	54.0	41.6	5.3	0.556
61	TCU129	23.878	120.684	11.9	6.2	D	999.2	78.1	64.0	6.0	0.599
62	TCU136	24.260	120.651	46.8	11.3	C	206.0	63.3	40.0	5.3	0.594
63	TCU138	23.922	120.595	21.9	15.2	D	214.7	39.6	42.3	5.4	0.584
64	TCU140	23.958	120.359	46.1	39.4	E	71.3	25.2	14.7	4.4	0.438
65	TCU141	23.834	120.464	34.3	28.0	E	93.3	46.0	20.3	4.8	0.514
66	TCU145	23.942	120.337	48.9	41.8	E	74.7	31.3	13.1	4.4	0.424
Hanging wall Stations											
1	HWA002	23.601	121.512	78.1	53.1	C	91.7	12.0	9.4	4.2	0.354
2	HWA005	23.661	121.414	66.4	43.8	D	155.6	19.4	21.9	4.8	0.404
3	HWA006	23.673	121.417	66.3	44	D	107.4	12.0	9.2	4.3	0.403
4	HWA015	23.973	121.563	77.8	49.5	D	109.1	18.5	17.7	4.7	0.347
5	HWA016	23.965	121.560	78.3	50.5	D	103.8	16.4	16.0	4.6	0.348
6	HWA017	23.948	121.547	76.0	49.0	D	86.7	12.2	12.1	4.4	0.353
7	HWA020	23.814	121.433	64.7	44.7	D	72.6	13.5	11.1	4.3	0.402
8	HWA029	23.937	121.571	78.9	52.4	D	95.6	17.3	16.9	4.7	0.342
9	HWA030	23.785	121.449	66.7	46.3	D	84.3	14.4	14.2	4.4	0.393
10	HWA031	23.766	121.493	71.4	50.4	D	112.0	20.1	21.2	4.8	0.370
11	HWA032	23.711	121.414	64.6	43.3	D	159.9	24.3	11.1	4.4	0.407
12	HWA033	23.686	121.474	71.5	49.2	C	185.2	21.6	22.7	5.0	0.376
13	HWA034	23.591	121.377	66.1	40.9	D	154.9	14.6	14.0	4.7	0.420
14	HWA035	23.730	121.445	66.4	45.4	D	81.4	11.7	9.2	4.2	0.392
15	HWA043	23.709	121.540	77.3	55.1	D	83.8	15.8	9.4	4.1	0.346
16	HWA044	23.654	121.528	77.6	54.2	D	83.7	10.1	8.4	4.1	0.349
17	HWA048	24.011	121.572	80.4	50.4	D	169.9	23.8	28.4	4.9	0.345
18	HWA049	23.995	121.560	78.6	49.4	D	104.8	24.6	22.7	4.8	0.351
19	HWA051	23.870	121.548	76.2	53.4	D	176.9	23.7	24.1	5.1	0.350
20	HWA056	24.180	121.508	80.3	42.7	B	119.0	11.4	8.5	4.2	0.383
21	HWA058	23.966	121.492	70.7	43.3	?	125.5	13.0	12.9	4.4	0.380
22	HWA059	23.871	121.508	71.4	49.2	?	150.4	18.1	20.7	4.9	0.368
23	IES180	24.205	121.441	74.8	37.2	B	141.4	17.9	17.0	4.3	0.418
24	IES183	24.021	121.109	35.3	20.2	B	563.9	64.6	79.5	5.9	0.534
25	IES184	24.083	121.167	44.0	22.1	B	245.1	79.6	43.6	5.4	0.523
26	IES192	24.310	121.285	69.6	27.6	B	329.2	23.7	18.2	4.7	0.484
27	IES193	24.249	121.236	61.2	24.1	B	330.4	37.3	47.9	5.4	0.510

Table 1 (*continued*)

No.	Station code	Latitude (°N)	Longitude (°E)	r_{epi} (km)	r_{seis} (km)	Soil type	PGA_R (cm/s^2)	PGV_R (cm/s)	SI (cm/s)	I_{JMA}	$Y\cos(\phi)$
28	TCU052	24.198	120.740	37.9	3.4	D	504.2	265.7	136.7	6.3	0.596
29	TCU068	24.278	120.766	46.3	3.1	D	460.0	384.4	82.1	6.1	0.593
30	TCU071	23.986	120.788	13.9	4.9	D	813.6	84.5	68.4	5.9	0.590
31	TCU072	24.039	120.858	20.6	7.9	D	466.5	89.8	65.1	5.9	0.581
32	TCU074	23.961	120.962	20.0	13.8	D	609.9	76.6	88.9	6.0	0.563
33	TCU078	23.812	120.846	7.1	8.3	D	471.1	45.9	47.8	5.6	0.582
34	TCU079	23.840	120.894	9.9	11.0	D	582.5	67.5	78.4	6.0	0.575
35	TCU084	23.883	120.900	10.5	11.4	?	984.0	125.3	161.0	6.5	0.574
36	TCU088	24.253	121.176	58.0	13.2	B	720.2	37.7	21.0	5.1	0.523
37	TCU089	23.904	120.857	7.5	8.3	C	365.5	46.5	32.7	5.3	0.581
Stations on site off the end of the fault											
1	IES171	23.071	120.659	89.2	55.2	B	48.2	8.1	6.3	3.5	N/A
2	IES173	23.258	120.813	67.0	34.5	B	167.4	7.9	8.2	4.2	N/A
3	IES174	23.277	120.902	65.6	33.2	B	165.1	12.2	12.0	4.5	N/A
4	IES188	24.486	121.527	100.8	52.5	B	80.4	12.8	10.9	4.3	N/A
5	IES189	24.481	121.441	94.3	46.2	B	76.4	12.6	8.4	4.2	N/A
6	TCU035	24.616	120.788	83.7	36.4	D	164.2	34.7	27.4	4.8	N/A
7	TCU131	24.567	120.817	78.3	32.0	D	167.2	46.7	27.0	4.8	N/A

r_{epi} and r_{seis}: Epicentral distance and shortest distance to the seismogenic part of the Chelungpu fault, respectively.
Soil type: Site-classification of Taiwan free-field strong-motion stations by Lee *et al.* [39] compatible with the provisions of the 1997 National Earthquake Hazard Reduction Program (NEHRP) and Uniform Building Code (UBC), respectively.
?: The site condition is questionable [39].
PGA_R and PGV_R: The PGA and PGV are defined as the maximum of the resultant of the two horizontal components as originally recorded.
SI: Spectrum Intensity (cm/s).
I_{JMA}: Japan Meteorological Agency (JMA) instrumental seismic intensity.
$Y\cos(\phi)$: Directivity function.
N/A: Not applicable.

Table II. Regression coefficients for ground motion parameters in the 1999 Chi-Chi, Taiwan earthquake.

Hanging wall	b_0	b_1	b_2	d (km)	ε
PGA_R	4.757	−0.01288	−0.89	69.2	0.135
PGA_R	2.842	0.0	−0.98	0.0	0.163
SI	3.162	−0.00463	−0.99	11.5	0.202
I_{JMA}	8.421	−0.00780	−1.98	10.0	0.350
Footwall					
PGA_R	3.674	−0.00096	−0.98	6.0	0.178
PGV_R	2.982	−0.00898	−0.86	75.1	0.199
SI	3.064	−0.01112	−0.72	57.1	0.162
I_{JMA}	7.945	−0.01293	−1.66	17.5	0.315

mean predicted attenuation of PGA_R, PGV_R, SI, and I_{JMA} for the footwall stations are almost characterized by constant values at a closest distance of 3 km to the seismogenic part of the fault plane as 550 cm/s^2, 90 cm/s, 56 cm/s, and 5.7 in the JMA scale, respectively. However, in the case of hanging wall stations the near-source effect cannot be observed for PGV_R, but PGA_R, SI, and I_{JMA} are saturated to 670 cm/s^2, 100 cm/s, and 6.2 in the JMA scale, respectively, at the source region ($r = 3$ km). For the hanging wall stations, significantly large ground motion variations are observed compared to those at the footwall stations with the same closest distance. Although the mean resulting attenuation curves almost fit the data in the near-fault rupture regions, still the scatterings of ground motion parameters due to local site conditions as well as hanging wall and directivity effects are observed [27, 36].

HANGING WALL AND FOOTWALL EFFECTS

Residual distribution

Recent empirical and numerical models indicated that the peak ground accelerations (PGA) on the hanging wall and footwall sites from thrust earthquakes are likely to show a systematic difference [18]. Based on the geometry of dipping faults, the ground motion at the hanging wall sites has a larger value than that on the footwall sites at the same seismogenic distance. Figure 4 shows the mean predicted PGA_R by the Chi-Chi earthquake-specific attenuation relationships for all the selected near-field, hanging wall and footwall stations. The hanging wall and footwall effects are demonstrated by examining the residuals from the mean Chi-Chi earthquake-specific attenuation relation. The PGA_R residuals for recording stations on the hanging wall and footwall are shown in Figure 5. The footwall stations are plotted on negative distances to distinguish them from the hanging wall sites. The PGA residuals on the hanging wall show a positive bias trend for the seismogenic distance range of 3 to 30 km with the mean bias of 0.43 and the standard deviation of 0.058. However, for the footwall sites, there is no significant bias over the same distance range with the mean residual of 0.03 ± 0.006 (Figure 5). For the 1999 Chi-Chi earthquake the maximum difference in the residual on the hanging wall and footwall over this distance range is observed at about 0.50, which means the expected PGA values on the hanging wall are 50% larger than those values on the footwall side for the same seismogenic distances.

Empirical model approach of the hanging wall and footwall effects

In order to model the residual trends on both the hanging wall and footwall sites, we introduce an empirical approach. The difference between the mean predicted Chi-Chi earthquake-specific attenuation relationship and the mean attenuation relations for the hanging wall and footwall sites could represent the general trends of the hanging wall and footwall, respectively. As can be seen from Figure 5, the continuous empirical-residual curve (thin line) for the hanging wall reaches its maximum value at 0.47 over the seismogenic distances of 5 to 30 km. However, the empirical residual function for the footwall sites does not represent a significant trend. It shows an average residual trend of 0.04 over the seismogenic distance to the fault plane. For the distance dependence of PGA residuals in the 1999 Chi-Chi earthquake on the hanging

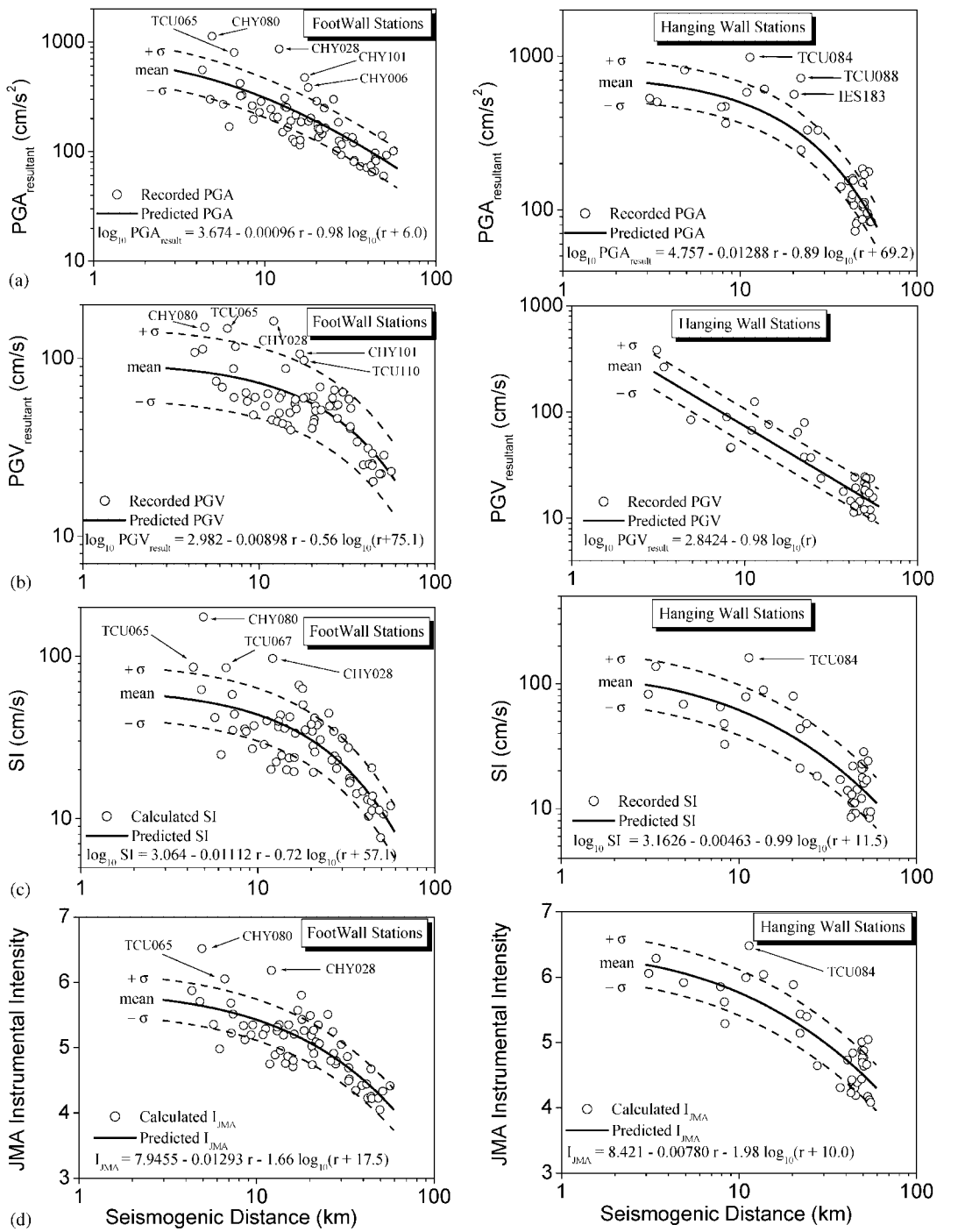

Figure 3. Predicted: (a) PGA; (b) PGV; (c) SI; and (d) I_{JMA} by the attenuation relationship for the (left) footwall and (right) hanging wall sites in the 1999 Chi-Chi, Taiwan earthquake.

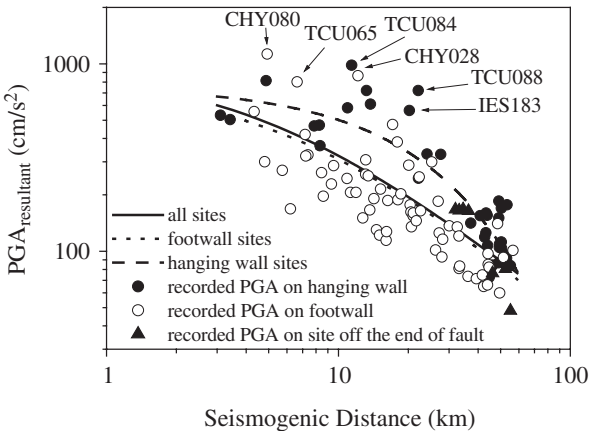

Figure 4. Mean predicted PGA for all the selected near-field stations (thick line), hanging wall stations (dash line), and footwall stations (dot line), respectively. Symbols are the recorded PGA on the footwall (open circle), hanging wall (solid circle), and site off the end of fault stations (triangle).

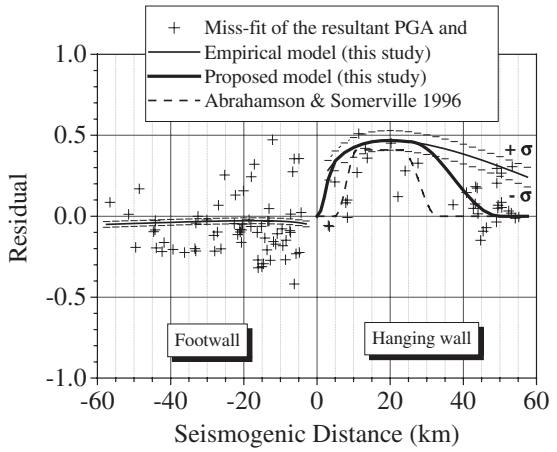

Figure 5. Empirical model of the PGA residuals on the hanging wall and footwall derived from the 1999 Chi-Chi, Taiwan earthquake records.

wall (hatch dot and continuous thin line), we introduce a piecewise continuous functional form represented by Equation (2). The proposed empirical model derived from the Chi-Chi earthquake records is used for the most affected seismogenic distance range of 5 to 25 km. A cosine function proposed by Abrahamson and Somerville [18], which gives a smooth decay with increasing source-to-site distance, are used for the seismogenic distances of 0 to 5 km and 25 to 50 km, respectively. Based on the trends in the residuals, the distance-dependent

Table III. Boundary distance and initial parameters for the Chi-Chi earthquake hanging wall effects on peak ground acceleration.

Parameter	Value
x_1	0 km
x_2	5 km
x_3	25 km
x_4	50 km
c_1	0.34
c_2	0.46

hanging wall effect can be written as

$$\mathrm{HW}_{\mathrm{effect}} = \begin{cases} \dfrac{c_1}{2}\left[\cos\left(\dfrac{\pi(r-x_1)}{x_2-x_1}+\pi\right)+1\right] & x_1 < r < x_2 \\ \mathrm{Prd}(r)_{\mathrm{Hanging\_wall}} - \mathrm{Prd}(r)_{\mathrm{All}} & x_2 \leqslant r \leqslant x_3 \\ \dfrac{c_2}{2}\left[\cos\left(\dfrac{\pi(r-x_3)}{x_4-x_3}\right)+1\right] & x_3 < r < x_4 \end{cases} \quad (2)$$

in which $\mathrm{HW}_{\mathrm{effect}}$ (r) is the hanging wall effect function and Prd (r) is the mean predicted Chi-Chi earthquake-specific attenuation curve. The boundary distances, x_1, x_2, x_3, and x_4, were determined using the residual-trend distributions and the initial values for the cosine function, c_1 and c_2, were assigned from the proposed empirical curve (Table III). The result obtained (see the thick line in Figure 5) shows a similar trend with the result by Abrahamson and Somerville [18], which was derived from the thirteen records on hanging wall sites during the 1994 Northridge earthquake and supplemented by the United States and worldwide data with the reverse/oblique earthquakes. The proposed empirical model for PGA on the hanging wall showed about 46% to 50% higher values than the mean attenuation for all the sites over the limited range of seismogenic distance from 5 to 25 km. In contrast, the proposed model for PGA on the footwall does not show a significant difference from the mean attenuation relation in the 1999 Chi-Chi, Taiwan earthquake.

EMPIRICAL DIRECTIVITY MODEL

The directivity and ground motion parameters for the development of the spectral amplification factor in the 1999 Chi-Chi, Taiwan earthquake were calculated using the model by Somerville *et al.* [1].

Directivity model parameters

The rupture directivity parameters such as the width ratio (Y, the fraction of the fault up-dip that ruptures towards a site), the zenith angle (ϕ) between the fault plane and ray path propagation to a site, and the average two horizontal components spectral acceleration were calculated (Table I). The schematic definition of the rupture directivity parameters, Y and

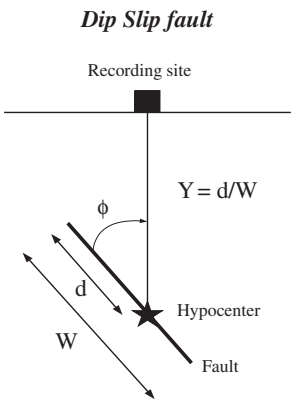

Figure 6. Definition of rupture directivity parameters (after Somerville *et al.* [1]).

ϕ, for the dip-slip Chelungpu fault is shown in Figure 6. The Y and ϕ mainly control the amplitude variation due to rupture directivity. In order to retain the magnitude and distance dependence, the variation of the directivity function, $Y\cos(\phi)$, with respect to the residuals between the recorded average horizontal spectral acceleration, calculated by the empirical model, is demonstrated in Figure 7 for the selected structural periods. As for the generic attenuation relation, the empirical model of Abrahamson and Silva [20], which considered the hanging wall effect and the style-of-faulting factor as well as site classifications, accommodating non-linear soil response effects, is used [37]. Their data set consists of 58 earthquakes from the United States supplemented by worldwide data. The recording sites off the end of the Chelungpu fault were excluded from the data set (hatched area in Figure 8). The selected recording stations from this earthquake, the surface projection of the rupture plane by the USGS and the sites off the end of the fault [1] are shown in the same figure.

Spatial variation in residual response spectra

The residual between recorded and model spectral acceleration is only a function of the distance width ratio, Y, and the zenith angle, ϕ. The dependence of the directivity model on these two parameters was examined by a regression analysis for the current data set. The residuals were fit using the directivity function form:

$$R = C_1 + C_2 Y\cos\phi + \sigma \tag{3}$$

where R is the residual of the natural logarithm of the spectral acceleration at a given period, C_1 and C_2 are period-dependent coefficients to be determined by linear regression, and σ represents the intra-event standard deviation. In order to remove bias between our data set and those used by Abrahamson and Silva [20] before performing a regression analysis the C_1 was reduced using a constants value that was obtained while setting C_2 to zero. The obtained coefficients are plotted as a function of period in Figure 9. Although there are small variations in the obtained coefficients, the general trends of regression coefficients, smoothed by a polynomial fitting, are in good agreement with the results of Somerville *et al.* [1]. As seen

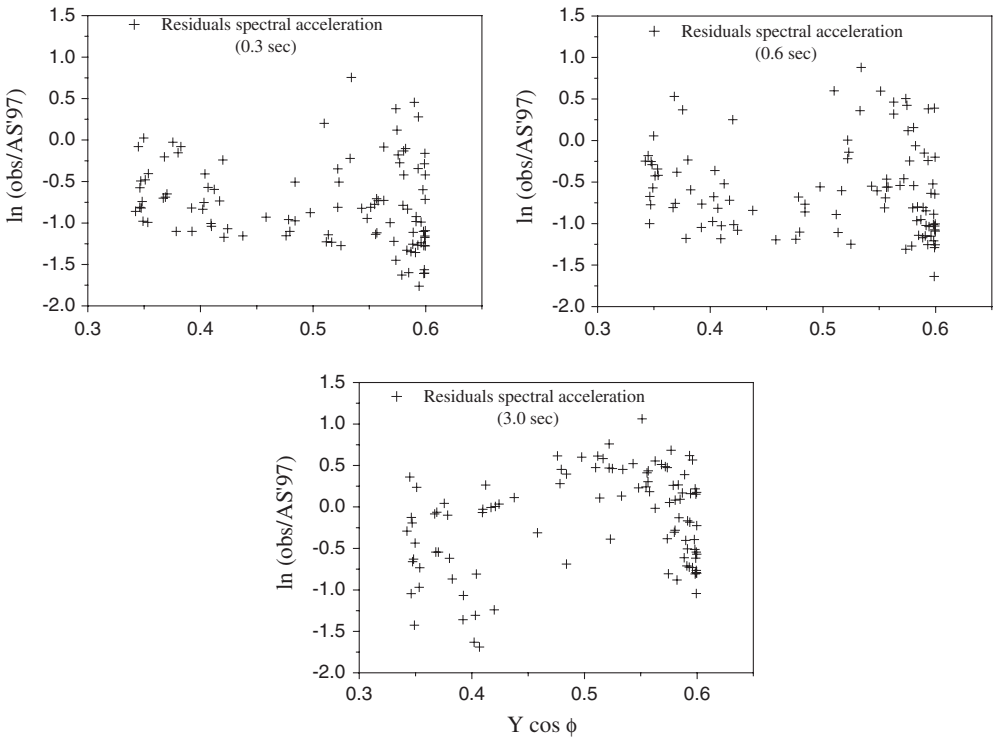

Figure 7. Residuals between the recorded average horizontal spectral acceleration and the Abrahamson and Silva [20] model as a function of the directivity parameter for three periods.

from Figure 9, the constant term, C_1, has an inverse dependence on the amplitude residual, which indicates a reduction in the base ground motion level, while increments are added at the recording stations having directivity effects [1]. The directivity function coefficient, C_2, shows a significant amplification for the periods greater than 0.6 s.

Magnitude- and distance-independent spectral directivity factor

The dependence of the spectral amplification factor on the directivity function ($Y \cos \phi$) and structural period for the thrust faulting system is shown in Figure 10. The directivity effects start from 0.6 s and increase with period (Table IV). For the dip-slip faulting, the maximum directivity condition ($Y \cos \phi = 1$) causes the amplitude to be about 1.8 times larger than the average at 2 s, which is two times larger than the corresponding amplification factor obtained by Somerville *et al.* [1], as shown in Table IV. For various structural periods, the spatial variation in the directivity factor during the 1999 Chi-Chi earthquake was evaluated for the near-fault stations as shown in Figure 11. From this figure, it can be seen that the rupture directivity effects are larger and almost concentrated on the top edge of the surface-faulting region. Although relatively small directivity factors registered for the period ranges of 0.6 s to 1.0 s due to the low-angle Chelungpu faulting system and the shallow focal-depth of this event

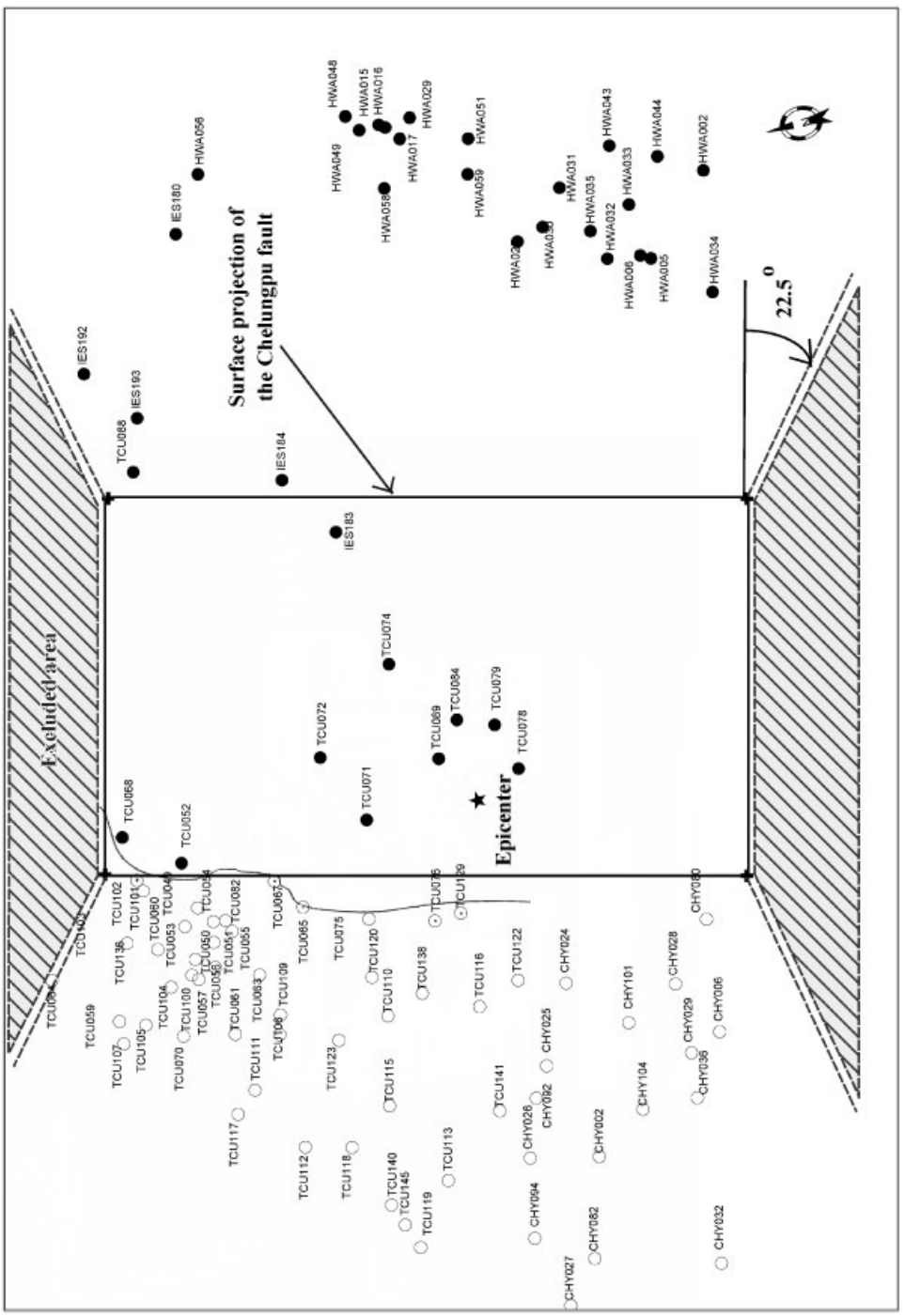

Figure 8. Nearby recording stations in the 1999 Chi-Chi, Taiwan earthquake. Surface projection of the rupture plane by USGS, epicenter, footwall stations (open circle), hanging wall stations (solid circle), and sites off the end of the Chelungpu fault (hatched area), which are excluded from data set.

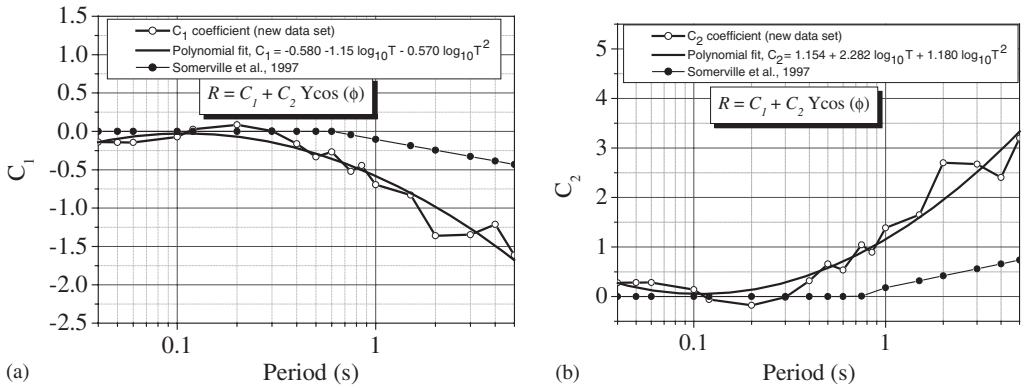

Figure 9. Results of the linear regression analysis for the directivity model: (a) intercept; and (b) directivity function coefficients. The obtained results of this study (open-dot line) are compared with the result by a previous study (solid-dot lines).

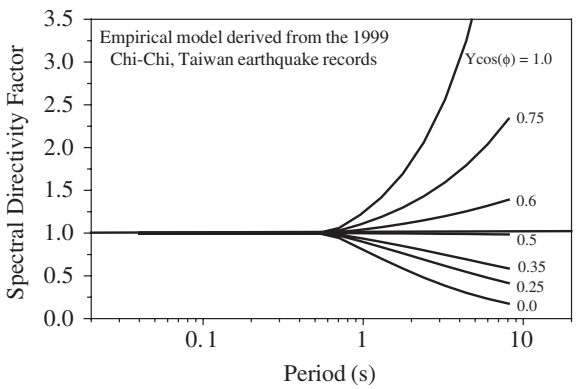

Figure 10. Empirical model of the response spectral amplitude ratio derived from the 1999 Chi-Chi, Taiwan earthquake, indicating its dependence on the period and directivity function.

[16, 38], significant rupture-directivity attributions have been observed for the longer periods. The spectral directivity factor results in 30% amplification at the period of 5.0 s (Figure 11). Since the spectral directivity amplification factor is distance- and magnitude-independent, it can be used for other attenuation relations and structural design evaluation studies especially for shallow large-magnitude events.

Examination of the proposed model in residual variation

The spectral acceleration variation due to the hanging wall/footwall effect was evaluated for several structural periods (Figures 12(a)–(d)) in the Chi-Chi earthquake. As can be seen from these figures, for the short-period intervals up to 0.6 s, the general trend of the residuals is

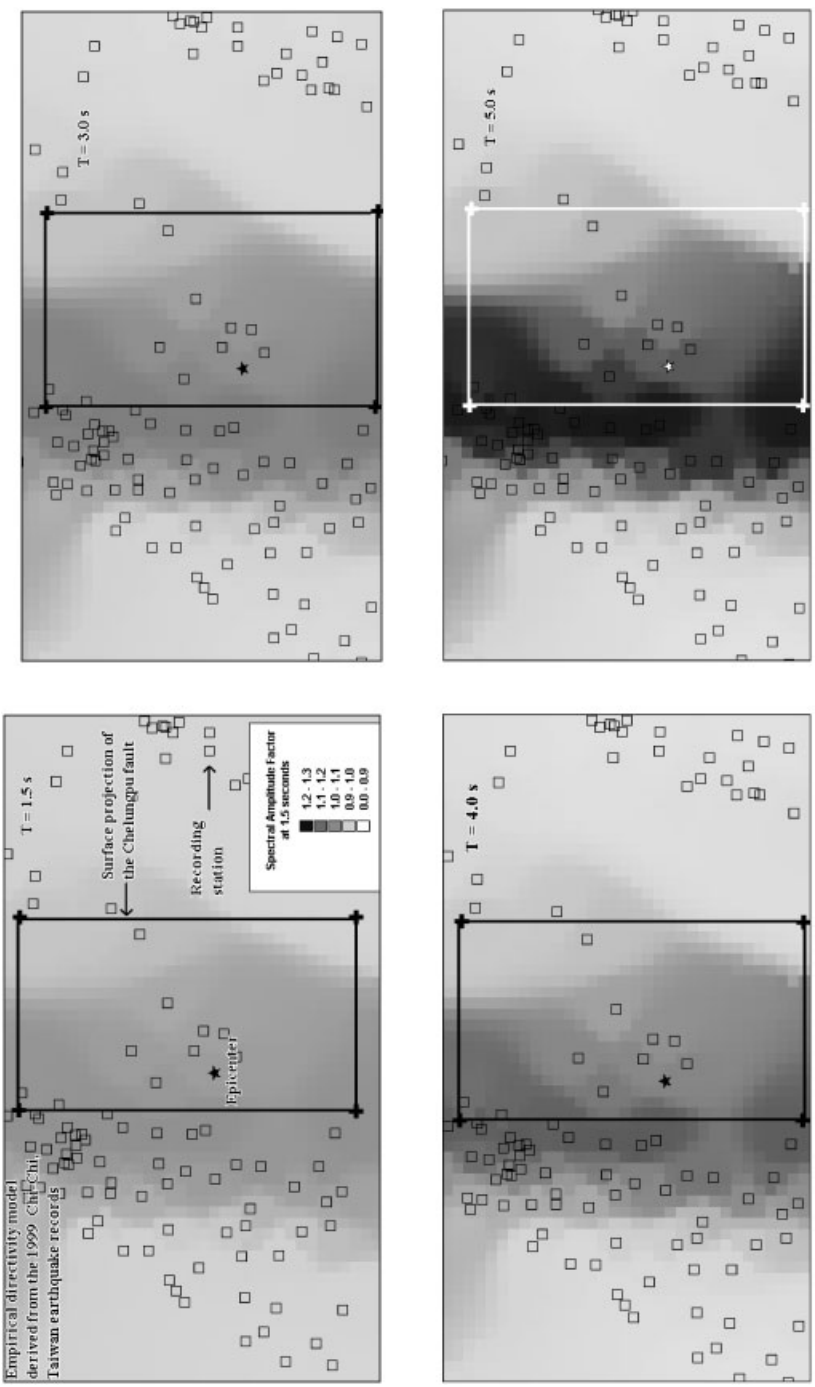

Figure 11. Illustration of spatial variation due to long-period directivity factor, using the proposed spectral directivity model for several periods during the 1999 Chi-Chi, Taiwan earthquake.

Table IV. Empirical-model results for spatial variation of spectral amplification due to directivity effects derived from the 1999 Chi-Chi Taiwan earthquake records.

Period (s)	C_1	C_2	C_1^*	C_2^*	σ	τ	σ^*	τ^*
0.6	0.000	0.000	0.000	0.000	0.395	0.000	0.514	0.000
0.75	−0.129	0.255	−0.045	0.008	0.393	0.000	0.549	0.000
1.0	−0.278	0.552	−0.104	0.178	0.356	0.000	0.540	0.001
1.5	−0.448	0.890	−0.186	0.318	0.325	0.000	0.568	0.169
2.0	−0.640	1.269	−0.245	0.418	0.331	0.000	0.602	0.260
3.0	−0.852	1.690	−0.327	0.559	0.298	0.000	0.690	0.211
4.0	−1.085	2.152	−0.386	0.659	0.420	0.000	0.616	0.360
5.0	−1.339	2.655	−0.431	0.737	0.638	0.000	0.634	0.522

C_1 and C_2: Period dependence intercept and directivity function coefficients.
σ: Intra-event standard deviation.
τ: Inter-event standard deviation.
*: The directivity model results of Somerville *et al.* [1].

consistent with the PGA residuals (Figures 12(a) and (b)). However, owing to the rupture directivity effect, especially at the footwall side, there is a change in the trend for the long-period motion. Figures 12(c) and (d) show the results of those adjustments for the rupture directivity effect using the proposed spectral amplification model. The residual distributions on the footwall and hanging wall sides for the PGV_R, SI, and I_{JMA} were also calculated (Figures 13(a)–(c)). From Figures 13(a) and (b) the PGV_R and SI residuals show a positive bias trend (hatch sign). This trend distribution close to the up-dip region of the Chelungpu fault can be explained by the rupture directivity effect [18, 38]. Thus, the observed residual trends were corrected for the long-period (i.e., 2.0 s) rupture-directivity effect (open circle) using the proposed model (Figures 13(a) and (b)). However, there is no significant bias for the I_{JMA} residuals over the same near-fault distance ranges (Figure 13(c)). Therefore, the hanging wall/footwall and rupture directivity effects do not have a significant influence on the I_{JMA} residual distributions. In this sense, the I_{JMA} might reflect the damage status more than PGV and SI did in the Chi-Chi earthquake.

CONCLUSIONS

In this study, empirical models representing the near-fault hanging wall and directivity effects that feature spatial variations in ground motions during the 1999 Chi-Chi, Taiwan earthquake were proposed using the comprehensive near-field strong ground motion records. The major results obtained are summarized as follows:

(1) Since there were a sufficient number of the near-field data registered during this damaging earthquake, Chi-Chi earthquake-specific attenuation relationships for the strong motion parameters were developed. It is preferable to use an event-specific attenuation relation since it does not include the influence of inter-event variability when capturing systematic near-fault features.
(2) At a shortest distance of 3 km to the seismogenic part of the rupture plane, the mean resulting attenuation curves for the PGA, SI, and I_{JMA} were found to be the constant

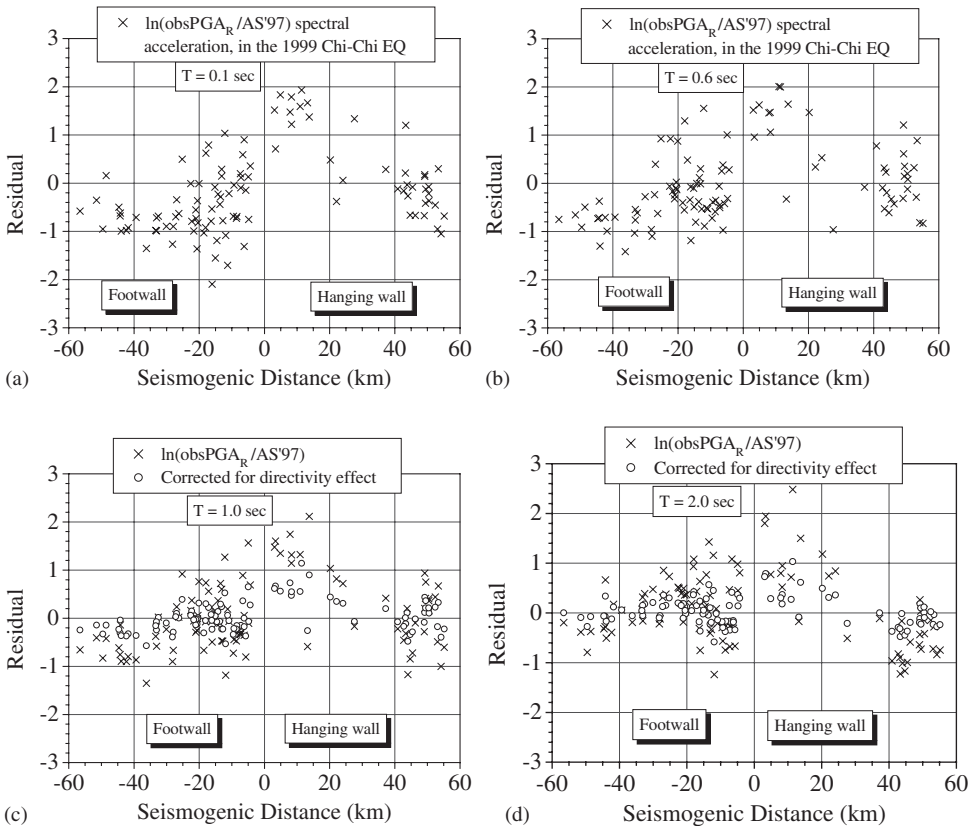

Figure 12. Residual spectral acceleration variation due to the hanging wall/footwall effect during the Chi-Chi earthquake. Residual variation at (a) 0.1 s and (b) 0.6 s, and those corrected for the directivity effect at (c) 1.0 s, and (d) 2.0 s by the proposed spectral model.

values in the source region. However, owing to the large variation in PGV at the northern part of the Chelungpu thrust (hanging wall sites), the near-source saturation effect for PGV was not observed.

(3) The systematic differences in ground motion parameters in the hanging wall and footwall sites are observed from the mean predicted attenuations. We introduced an empirical hanging wall model for PGA, using the residual of the obtained attenuation relationships. The new empirical model for the PGA on the hanging wall indicates 46% to 50% higher values than the mean predicted ones over the near-field range of 5 to 25 km. The suggested empirical hanging wall model was confirmed by the result of Abrahamson and Somerville.

(4) An empirical directivity model of the response spectral amplitude ratio was proposed assigning magnitude- and distance-independence for the fault geometry model of the Chelungpu fault. The proposed model shows a larger spectral amplification factor for the dip-slip faulting system than the result of Somerville *et al.*

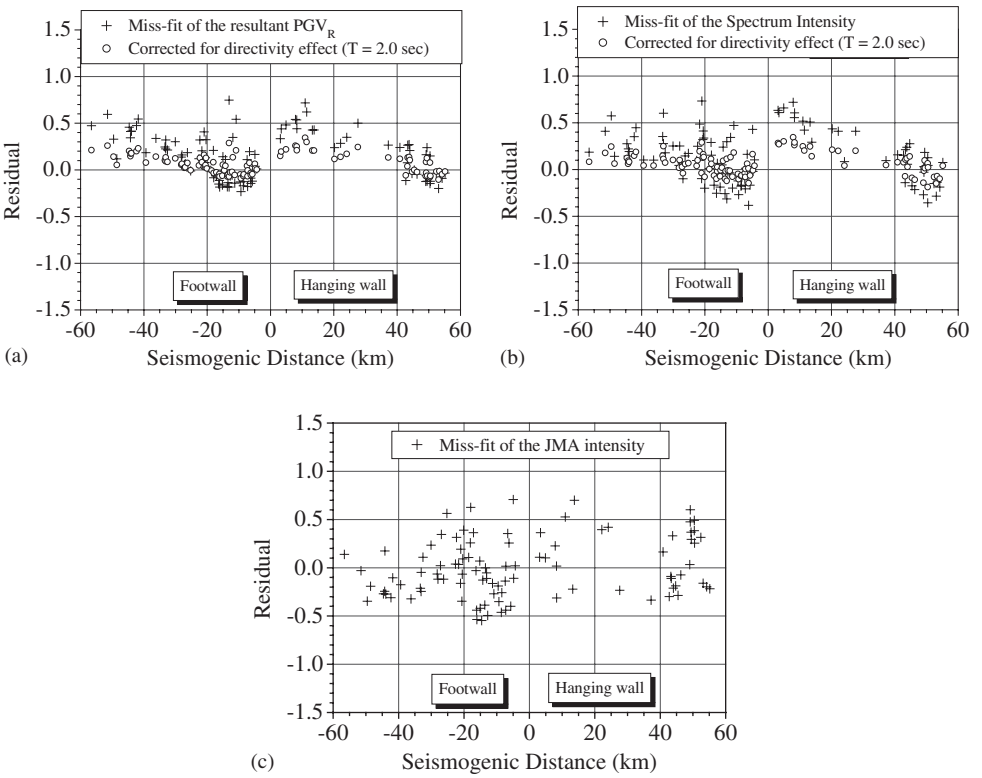

Figure 13. Comparison of hanging wall/footwall effect on: (a) PGV; (b) SI; and (c) I_{JMA} residuals from the Chi-Chi, Taiwan earthquake. The residual of PGV and SI are corrected for directivity effect at 2.0 seconds (circle) using the proposed model.

(5) During the Chi-Chi earthquake, the maximum spectral directivity factors have been registered in the top-edge area located around the surface exposure of the Chelungpu fault, in the range of 1.1 to 1.3 for the structural periods of 0.6 s to 5.0 s.

The proposed empirical spectral amplification model incorporating near-fault effects can be easily implemented into attenuation relations, seismic hazard studies, and the seismic design of long-period structures for shallow large-magnitude events in the regions with a dip-slip faulting system.

ACKNOWLEDGEMENTS

The authors would like to thank the Seismological Center, Central Weather Bureau (CWB), Taipei, Taiwan, for providing the digital strong motion records of the 1999 Chi-Chi, Taiwan earthquake. We gratefully appreciate the useful comments of two anonymous reviewers.

REFERENCES

1. Somerville P, Smith, NF, Graves RW, Abrahamson NA. Modification of empirical strong ground motion attenuation relations to include the amplitude and duration effects of rupture directivity. *Seismological Research Letters* 1997; **68**(1):199–222.
2. Aagaard BT, Hall JF, Heaton TH. Characterization of near-source ground motions with earthquake simulations. *Earthquake Spectra* 2001; **17**(2):177–207.
3. Brune JN. Shattered rock and precarious rock evidence for strong asymmetry in ground motions during thrust faulting. *Bulletin of the Seismological Society of America* 2001; **91**(3):441–447.
4. Chen C-H, Wang W-H, Teng TL. 3-D velocity structure around the source area of the 1999 Chi-Chi, Taiwan earthquake: before and after the mainshock. *Bulletin of the Seismological Society of America*, 2001; **91**(5):1013–1027.
5. Hayashi K, Burns DR, Toksoz MN. Discontinuous-grid finite-difference seismic modeling including surface topography. *Bulletin of the Seismological Society of America* 2001; **91**(6):1750–1764.
6. Boatwright J, Boore DM. Analysis of the ground accelerations radiated by the 1980 Livermore Valley earthquakes for directivity and dynamic source characteristics. *Bulletin of the Seismological Society of America* 1982; **72**(6):1843–1865.
7. Singh JP. 1982. Directivity evidence from the August 6, 1979 Coyote Lake earthquake. *Proceedings of the Conference on Earthquake Hazards in the Eastern San Francisco Bay Area, Hayward, California.* California Division of Mines and Geology. Special Publication vol. 62, 1982; 24–27.
8. Wald DJ, Heaton TH, Helmberger DV. Rupture model of the 1989 Loma Prieta earthquake from the inversion of strong motion and broadband teleseismic data. *Bulletin of the Seismological Society of America* 1991; **81**:1540–1572.
9. Wald DJ, Kanamori H, Helmberger DV, Heaton TH. Source study of the 1906 San Francisco earthquake. *Bulletin of the Seismological Society of America* 1993; **83**:981–1019.
10. Velasco AM, Ammon CJ, Lay T. Empirical Green function deconvolution of broadband surface waves: Rupture directivity of the 1992 Landers, California ($M_w = 7.3$) earthquake. *Bulletin of the Seismological Society of America* 1994; **84**:735–750.
11. Hall JF, Heaton TH, Halling MW, Wald DJ. Near-source ground motions and its effects on flexible buildings, *Earthquake Spectra* 1995; **11**:569–606.
12. Pitarka A, Irikura K, Iwata T, Sekiguchi H. Three-dimensional simulation of the near-fault ground motion for the 1995 Hyogo-ken Nanbu (Kobe), Japan, earthquake. *Bulletin of the Seismological Society of America* 1998; **88**(2):428–440.
13. Somerville P. Characterized of near fault ground motions. *U.S.-Japan Workshop*: *Effects of Near-Field Earthquake Shaking*, PEER and ATC, 2000; **5**:1–8.
14. Wang W-H, Chen C-H. Static stress transferred by the 1999 Chi-Chi, Taiwan, earthquake: effects on the stability of the surrounding fault systems and aftershock triggering with a 3D fault-slip model. *Bulletin of the Seismological Society of America* 2001; **91**(5):1041–1052.
15. Lee WHK, Shin TC. Strong-motion instrumentation and data. *Earthquake Spectra* (special issue on the Chi-Chi, Taiwan earthquake reconnaissance report) 2001; **17**:5–18.
16. Yagi Y, Kikuchi M. Source rupture process of the 1999 Chi-Chi, Taiwan earthquake. *http://wwweic.eri.u-tokyo.ac.jp/yuji/taiwan/taiwan.html*, 1999.
17. Lee WHK, Shin TC, Kuo KW, Chen KC, Wu CF. CWB free-field strong ground-motion data from the 21 September, Chi-Chi, Taiwan, earthquake. *Bulletin of the Seismological Society of America* 2001; **91**(5):1370–1376.
18. Abrahamson NA, Somerville PG. Effects of the hanging wall and footwall on ground motions recorded during the Northridge earthquake. *Bulletin of the Seismological Society of America* 1996; **86**(1B):S93–S99.
19. Zhao D, Kanamori H, Negishi H, Wiens D. Tomography of the source area of the Kobe earthquake: evidence for fluids at the hypocenter. *Science* 1996; **274**:1891–1894.
20. Abrahamson NA, Silva WJ. Empirical response spectral attenuation relations for the shallow crustal earthquakes. *Seismological Research Letters* 1997; **68**(1):94–127.
21. Campbell KW. Near-source attenuation of peak horizontal acceleration. *Bulletin of the Seismological Society of America* 1981; **71**(6):2039–2070.
22. Sokolov V, Loh CH, Wen KL. Empirical models for the site- and region-dependent ground-motion parameters in the Taipei area. *Earthquake Spectra* 2001; **17**(2):313–332.
23. Boore DM. Effect of baseline corrections on response spectra for two recordings of the 1999 Chi-Chi, Taiwan, earthquake. *U.S. Geological Survey Open-file Report No. 99-545*, 1999.
24. Wen K-L, Peng H-Y, Tsai Y-B, Chen K-C. Why 1G was recorded at TCU129 site during the 1999 Chi-Chi, Taiwan, earthquake. *Bulletin of the Seismological Society of America* 2001; **91**(5):1255–1266.

25. Dalguer LA, Irikura K, Riera JD, Chiu HC. The importance of the dynamic source effects on strong ground motion during the 1999 Chi-Chi, Taiwan earthquake: brief interpretation of the damage distribution on buildings. *Bulletin of the Seismological Society of America* 2001; **91**(5):1112–1127.
26. Shabestari KT, Yamazaki F. Attenuation relationships of the ground motion parameters considering directivity effects in the 1999 Chi-Chi, Taiwan earthquake. *Proceedings of the Seventh National Conference on Earthquake Engineering*, 2002 CD-ROM.
27. Japan Meteorological Agency (JMA) Shindo wo Shiru (Note on the JMA seismic intensity). *Gyosei* 1996; 46-224 (in Japanese).
28. Yamazaki F. Seismic monitoring and early damage assessment system in Japan. *Progress in Structural Engineering and Materials* 2001; **3**:66–75.
29. Shabestari KT, Yamazaki F. A proposal of instrumental seismic intensity scale compatible with the MMI evaluated from three-component acceleration records. *Earthquake Spectra* 2001; **17**(4):711–723.
30. Katayama T, Sato N, Saito K. SI-sensor for the identification of destructive earthquake ground motion. *Proceedings of the 9th World Conference on Earthquake Engineering*. vol. VII, 1988; 667–672.
31. Shimizu Y, Watanabe A, Koganemaru K, Nakayama W, Yamazaki F. Super High-Density Realtime Disaster Mitigation System. *Proceedings of the 12th World Conference on Earthquake Engineering*, CD-ROM, 2000; 7.
32. Karim KR, Yamazaki F. Correlation of JMA instrumental seismic intensity with strong motion parameters. *Earthquake Engineering and Structural Dynamics* 2002; **31**(5):1191–1212.
33. Campbell KW. Predicting strong ground motion in Utah. *U.S. Geological Survey Open-file Report*, *No. 87-585*, 1987.
34. Fukushima Y, Tanaka T. A new attenuation relation for peak horizontal acceleration of strong ground motion in Japan. *Bulletin of the Seismological Society of America* 1990; **80**(4):757–783.
35. Boore DM, Joyner WB. The empirical prediction of ground motion. *Bulletin of the Seismological Society of America* 1982; **72**(6):43–60.
36. Shabestari KT, Yamazaki F. Hanging wall and footwall effects on ground motions: an empirical approach. *Proceedings of the 57th Annual Conference of JSCE*, I-885:1769-1770, CD-ROM, 2002.
37. Youngs RR. Soil amplification and vertical to horizontal ratios for analysis of strong motion data from active tectonic regions. Appendix, 2C in *Guidelines for Determining Design Basis Ground Motion Technical Report 102293*, vol. 2, 1993.
38. Somerville P. Magnitude scaling of near fault ground motions. *Proceedings of the International Workshop on Annual Commemoration of Chi-Chi Earthquake NCREE*, vol. I, 2000; 59–70.
39. Lee C-T, Cheng C-T, Liao C-W, Tsai Y-B. Site classification of Taiwan free-field strong-motion stations. *Bulletin of the Seismological Society of America* 2001; **91**(5):1283–1297.

